RESEARCH PAPER

Cascading Hybrid Metaheuristic Maximum Power Point Tracking for Photovoltaic Systems Under Partial Shading Conditions: A PSO–FPA–CSA–GWO Approach

Mohd Ahfaz Khan[1]*, Anurag S. D. Rai[2], Amol Barve[3]
[1,2,3]*Electrical Engineering Department, LNCT University, Bhopal, India.*
Corresponding author: Email: khan.ahfaz@gmail.com

Abstract

Partial shading conditions (PSC) distort the power–voltage characteristic of a photovoltaic (PV) array into a multi-peaked surface, causing single-stage maximum power point tracking (MPPT) methods to stagnate at local peaks. This paper proposes a cascading hybrid MPPT controller sequencing four metaheuristics with warm-started population handoff: particle swarm optimisation (PSO) for global exploration, the flower pollination algorithm (FPA) for neighbourhood narrowing, cuckoo search (CSA) for Lévy-flight refinement, and the grey wolf optimiser (GWO) for local convergence. The controller was evaluated on a single-diode model of a KC200GT module string under seven shading patterns, including two six-module patterns with competitive local peaks (peak ratio down to 0.56), against perturb-and-observe, incremental conductance, standalone PSO, and standalone GWO, over ten seeds per pattern (70 runs per method). The proposed cascade achieved a global-peak success rate of 100% (70/70 runs), a mean efficiency of 99.98% ± 0.03%, and a worst-case efficiency of 99.77%, versus 56.7% for standalone PSO and 51.3% for P&O/INC. Mean settling time was 0.042 s, matching the fastest single metaheuristic, with the lowest steady-state oscillation (0.058 W). A paired t-test confirmed a significant efficiency gain over GWO ($p = 3.2 \times 10^{-4}$) with significantly lower variance (Levene $p = 4.0 \times 10^{-4}$). An ablation study showed that removing CSA reduced the success rate to 98.6% and worst-case efficiency to 72.5%, confirming Lévy-flight refinement as the primary source of robustness. Staged metaheuristic composition, rather than any single algorithm, delivers consistently high tracking accuracy across a wide range of shading severities.

Keywords

How to cite this article: Mohd Ahfaz Khan, Anurag S. D. Rai, Amol Barve. Cascading Hybrid Metaheuristic Maximum Power Point Tracking for Photovoltaic Systems Under Partial Shading Conditions: A PSO–FPA–CSA–GWO Approach. Int J Drug Deliv Technol. 2026;16(80s):1426-1436. DOI: 10.25258/ijddt.16.80s.182.

1. Introduction

Photovoltaic (PV) generation is expanding rapidly as a low-carbon electricity source, but its energy yield is acutely sensitive to non-uniform irradiance. Partial shading, caused by clouds, adjacent structures, vegetation, or accumulated soiling, forces one or more series-connected modules in a string to conduct less current than their neighbours. Bypass diodes protect the shaded modules from hot-spot damage, but in doing so they reshape the array's power–voltage (P–V) characteristic into a curve with several local maxima and a single global maximum power point (GMPP). Locating the GMPP reliably, and doing so quickly enough to track a shading pattern that itself changes with passing clouds, is the central difficulty in maximum power point tracking (MPPT) under partial shading conditions (PSC).

Classical hill-climbing methods such as perturb-and-observe (P&O) and incremental conductance (INC) estimate the local gradient of the P–V curve and step the operating point accordingly [1,2]. Under uniform irradiance, where the P–V curve is unimodal, both methods converge reliably to within a few percent of the true maximum. Under PSC, however, the same gradient-following logic has no mechanism to distinguish a local peak from the GMPP: once P&O or INC settles at the nearest peak, it has no way to know that a taller peak exists elsewhere on the curve. Comparative studies consistently report this failure mode, with tracking efficiencies collapsing to 50–70% of the true GMPP whenever the array is shaded severely enough to create multiple competitive peaks [3,4].

Population-based metaheuristics address this shortcoming by sampling several candidate operating points simultaneously and exchanging information between them, which gives the search a mechanism to escape a local peak in favour of a better one. Particle swarm optimisation (PSO) was the first such method to be adapted for global MPPT [5]; PSO-based MPPT controllers apply the velocity-and-position update rule directly to the array duty cycle or voltage reference, using measured power as the fitness signal, and have demonstrated substantially higher GMPP-tracking success than P&O or INC under PSC [6]. The grey wolf optimiser (GWO) [7], which models the leadership hierarchy and encircling behaviour of a wolf pack, has likewise been adapted for MPPT and reported to converge faster than PSO on some shading patterns while requiring fewer tuned parameters [6].

Other bio-inspired swarm methods applied to PSC MPPT include artificial bee colony optimisation [8], the bat algorithm [9], firefly-based search [10], ant colony optimisation assisted P&O [11,12], the grasshopper optimisation algorithm [13], the whale optimisation algorithm combined with P&O refinement [14], falcon optimisation [15], and adaptive resistance-vector MPPT [16]. Each of these studies reports improved GMPP-tracking accuracy relative to classical methods on the specific shading patterns tested, but the algorithms are evaluated individually, and each retains characteristic weaknesses: PSO can prematurely converge when particle diversity collapses early; GWO's encircling mechanism narrows the search quickly, which speeds convergence but increases the risk of settling near, rather than at, a competitive local peak.

The flower pollination algorithm (FPA) [17], which alternates Lévy-flight-driven global pollination with local pollination between neighbouring solutions, has also been applied to PSC MPPT and shown to combine reasonably fast convergence with good GMPP accuracy [18]; adaptive variants that tune the switch probability during dynamic shading have improved robustness further [19]. The cuckoo search algorithm (CSA) [20], which uses Lévy flights to place new candidate solutions and probabilistically abandons the worst nests, has been reported to achieve very low steady-state oscillation and a low failure rate once tuned appropriately [21], including hardware-in-the-loop validation [22], combination with sliding-mode duty-cycle control [23], and dedicated schemes to reduce its exploration-phase tracking time [24].

Recognising that no single metaheuristic dominates on every shading pattern, several studies have combined two algorithms in sequence or in parallel. A widely cited example couples PSO for the initial global search with P&O for final fine-tuning, exploiting PSO's global reach and P&O's fast local convergence once the search is already close to the peak [25]. Fuzzy-adaptive PSO variants tune the inertia weight and acceleration coefficients online to reduce the sensitivity of PSO to its initial parameters [26], and PSO has also been used to tune the parameters of a sliding-mode controller downstream of the search [27]. Modified GWO variants adjust the convergence factor schedule to reduce overshoot [28], and more recent work has begun to combine metaheuristics with learning-based controllers, including fuzzy-deep-deterministic-policy-gradient hybrids [29] and artificial-neural-network-assisted P&O [30]. Comparative studies of PSO, genetic algorithms, and ant colony optimisation confirm that relative ranking among metaheuristics is itself shading-pattern-dependent [31], and recent comprehensive reviews of MPPT techniques for PSC catalogue dozens of individual and two-stage hybrid proposals without converging on a single dominant architecture [3,4].

Two gaps persist in this body of work. First, almost all reported hybrids combine exactly two algorithms — typically one global search phase and one local refinement phase. This leaves unexplored whether a longer cascade, in which each stage hands its population to a mechanistically different successor, can compound the exploration and exploitation strengths of more than two search behaviours without a proportional increase in tracking time. Second, robustness is rarely reported in a form that separates average-case accuracy from worst-case failure. A method that achieves 99% mean efficiency but occasionally collapses to 60% on a difficult shading pattern is materially less useful in a field deployment than one with a lower peak efficiency but no failures. Yet most published comparisons report only mean tracking efficiency and settling time. Few offer a success-rate metric, an ablation of which algorithmic component is responsible for robustness gains, or a statistical significance test against the strongest baseline.

This paper addresses both gaps by proposing and rigorously evaluating a four-stage cascading hybrid MPPT controller that sequences PSO, FPA, CSA, and GWO with warm-started population handoff between stages, and by reporting success rate, worst-case efficiency, and an ablation study alongside the conventional mean-efficiency and settling-time metrics. Unlike prior two-algorithm hybrids [25,26,28], which pair a single global-search phase with a single local-refinement phase, the proposed cascade interposes two additional, mechanistically distinct stages — FPA's pollination-driven neighbourhood narrowing and CSA's Lévy-flight nest refinement — between the initial PSO exploration and the final GWO convergence, and this paper demonstrates through ablation that it is specifically the CSA stage that supplies the robustness gain the cascade provides. The contributions of this paper are as follows.

- A four-stage cascading hybrid MPPT algorithm (PSO–FPA–CSA–GWO) is formulated with explicit warm-started state handoff between stages, requiring no additional tuning beyond the constituent algorithms' standard parameters.
- The algorithm is validated on a physically grounded single-diode model of a series string of industry-reference PV modules under seven shading patterns, two of which are six-module patterns engineered to produce closely competitive local peaks (top-two peak power ratio as low as 0.56), against perturb-and-observe, incremental

conductance, standalone PSO, and standalone GWO baselines.

- Across 70 independent seed-pattern runs, the proposed cascade attains a 100% global-peak convergence success rate, a mean tracking efficiency of 99.98% ± 0.03%, and a worst-case efficiency of 99.77%, compared with worst-case efficiencies of 56.7% for standalone PSO and 51.3% for P&O/INC, with the efficiency gain over GWO confirmed statistically significant (paired t-test, $p = 3.2 \times 10^{-4}$) alongside a significant reduction in outcome variance (Levene test, $p = 4.0 \times 10^{-4}$).
- An ablation study isolating each cascade stage identifies the Lévy-flight cuckoo search stage as the primary source of the cascade's robustness: removing it reduces the global-peak success rate from 100% to 98.6% and the worst-case efficiency from 99.77% to 72.5%, while removing the flower pollination stage alone has a comparatively small effect.

2. Problem Formulation

As identified in Section 1, the central obstacle to reliable MPPT under PSC is that the array power–voltage relationship becomes multimodal, and gradient-following controllers converge to whichever local mode is nearest their starting point rather than the global mode. This section restates that obstacle as a formal optimisation problem so that the cascading search strategy proposed in Section 3 can be described precisely.

2.1. Module and string model

Each PV module is represented by the single-diode equivalent circuit, in which the terminal current I is related to the terminal voltage V by

$$I = I_{ph} - I_0 \left[exp\frac{V + IR_s}{V_t} - 1 \right] - \frac{V + IR_s}{R_{sh}} \qquad (1)$$

where Iph is the photogenerated current, I0 the diode saturation current, Rs and Rsh the series and shunt resistances, and Vt = Ns a k T /q the modified thermal voltage of a module with Ns series-connected cells, ideality factor a, Boltzmann constant k, absolute temperature T, and elementary charge q. Parameters (Iph, I0, Rs, Rsh, Vt) are evaluated at each module's local irradiance Gk and cell temperature Tc following the standard temperature- and irradiance-scaling relations, so that a string of n series-connected modules under PSC has n generally distinct single-diode curves.

For a string current I common to all n series modules, each module k either sustains I on its own I–V curve, in which case its terminal voltage Vk(I) is obtained by inverting Equation (1), or the local irradiance is too low for module k to sustain I, in which case its bypass diode conducts and the module contributes a fixed forward-bias drop −Vd. The string terminal voltage and power are therefore

$$V(I) = \sum_{k=1}^{n} V_k(I), \quad P(I) = V(I) \cdot I \qquad (2)$$

Sweeping I from 0 to the largest short-circuit current among the n modules and evaluating Equation (2) at each point produces the array's P–V curve. Under uniform irradiance this curve is unimodal; under PSC, the piecewise switching between conducting and bypassed modules introduces up to n local maxima, of which only one is the GMPP.

2.2. Objective function, decision variable, and constraints

The controller's decision variable is the array terminal voltage V, realised in practice through the duty cycle D of a DC–DC boost converter interposed between the array and the load or grid-side inverter [35,36], with V and D related by the converter's steady-state voltage-gain characteristic. The MPPT problem is to find the voltage that maximises delivered power subject to the array's physical voltage limits:

$$V* = arg\,max\ P(V), \quad subject\ to\ 0 \le V \le V_{oc,str} \qquad (3)$$

where Voc,str is the open-circuit voltage of the string and P(V) is the power obtained by interpolating the sampled P–V curve of Equation (2) at V. Because P(V) is non-convex and possibly multimodal under PSC, Equation (3) cannot be solved by gradient ascent alone without risking convergence to a local maximum; Section 3 formulates a population-based cascade whose successive stages are chosen to first explore the full domain [0, Voc,str] broadly and then refine the estimate of V* with decreasing step size.

The controller is evaluated against two families of performance criteria that follow directly from Equation (3): accuracy criteria, which quantify how close the converged power P(Vfinal) is to the true optimum P(V*) obtained by exhaustive search (Section 4.4), and dynamic criteria, which quantify how many controller sampling steps are required to reach and remain within a tolerance band of P(V*).

3. System Model and Proposed Method

The proposed controller treats each stage of the search as a population of candidate voltages that is refined by a different metaheuristic update rule; the population and its associated fitness memory (best-known position per particle and globally) are carried across stage boundaries rather than re-initialised, so that later stages continue refining the search neighbourhood that earlier stages have already narrowed rather than starting over. Figure 1 shows the overall control architecture: the array voltage and current are sensed, the cascade controller computes a duty-cycle command for the boost converter, and the resulting operating point is fed back as the next fitness evaluation.

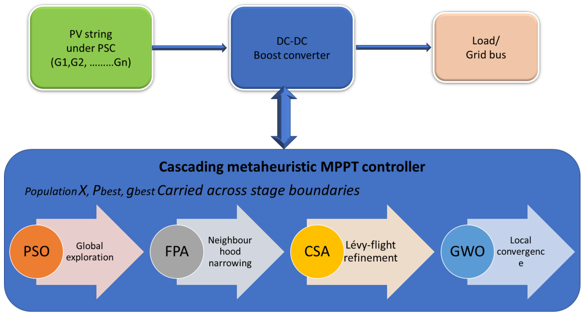

Fig. 1. Cascading metaheuristic MPPT controller architecture. Population state (X, personal bests, global best) is carried across the four stage boundaries.

3.1. Stage 1 — PSO global exploration

The cascade initialises Np candidate voltages Xi uniformly over [0, Voc,str] and updates each particle's velocity and position using the standard PSO rule,

$$v_i^{(t+1)} = wv_i^{(t)} + c_1r_1(p_{best,i} - X_i^{(t)}) + c_2r_2(g_{best} - X_i^{(t)}) \qquad (4)$$

with inertia weight w = 0.7 and acceleration coefficients c1 = c2 = 1.6, and velocities clamped to ±25% of Voc,str. Fitness is the interpolated array power P(Xi) from Equation (2). This stage occupies the first 20% of the iteration budget and is responsible for locating the general neighbourhood of the GMPP among the candidate peaks; its wide velocity limits favour exploration over precision.

3.2. Stage 2 — FPA pollination handoff

The population inherited from Stage 1 is refined using the flower pollination algorithm [17]. With switch probability p = 0.8, each candidate performs global pollination via a Lévy flight toward the current best position gbest,

$$X_i^{(t+1)} = X_i^{(t)} + L\cdot(g_{best} - X_i^{(t)}) \qquad (5)$$

where the step length L is drawn from a Lévy-stable distribution with exponent β = 1.5, generated by the Mantegna algorithm and scaled to 12% of Voc,str; otherwise, with probability 1 − p, the candidate performs local pollination by interpolating between two other randomly chosen population members. This stage runs from 20% to 45% of the iteration budget and narrows the search neighbourhood established in Stage 1 while retaining enough step-length diversity, through the heavy-tailed Lévy distribution, to jump between competing local peaks that lie close together in voltage.

3.3. Stage 3 — CSA nest refinement

The cuckoo search stage [20] performs a second, shorter-range Lévy-flight refinement centred on the incumbent best solution,

$$X_i^{new} = X_i^{(t)} + L'\cdot(X_i^{(t)} - g_{best}) \qquad (6)$$

with a step-length scale of 5% of Voc,str, followed by a probabilistic abandonment step in which a fraction pa = 0.25 of nests with the lowest fitness are discarded and re-seeded as Gaussian perturbations around gbest. This stage runs from 45% to 70% of the iteration budget. Its short-range Lévy flights are, as the ablation study in Section 5.5 shows, the primary mechanism by which the cascade escapes competitive local peaks that Stage 1–2 leave unresolved: because a fixed fraction of nests is discarded and redrawn every iteration regardless of the population's current fitness spread, the stage keeps probing near-tied peaks even after the population has nominally converged on one of them.

3.4. Stage 4 — GWO local convergence

The final stage applies the grey wolf optimiser [7]. The three fittest candidates are labelled α, β, and δ, and every candidate is updated toward a weighted combination of encircling positions around all three,

$$X_i^{(t+1)} = \frac{X_1 + X_2 + X_3}{3}, \quad X_1 = X\alpha - A\cdot|C\cdot X\alpha - X_i^{(t)}| \qquad (7)$$

with X2 and X3 defined analogously about Xβ and Xδ, and coefficients A = 2ar1 − a, C = 2r2 for independent random draws r1, r2 ∈ [0,1], where the convergence parameter a decays linearly from 2 to 0 over the stage's remaining iterations (70% to 100% of the budget). This shrinking encirclement radius delivers the final fine convergence to the GMPP with minimal residual oscillation. The stage boundaries were fixed a priori at 20/45/70/100% of the total budget and were not tuned against the evaluation shading patterns of Section 4; the same schedule is used for every pattern and every seed reported in Section 5, and Section 5.5 evaluates the sensitivity of the cascade's robustness to the presence or absence of individual stages.

4. Experimental Setup

4.1. Dataset and PV array model

All experiments use a physically grounded single-diode model of the Kyocera KC200GT module, a 54-cell polycrystalline module whose datasheet parameters (Voc = 32.9 V, Isc = 8.21 A, Vmp = 26.3 V, Imp = 7.61 A, Pmax = 200.1 W at standard test conditions) are a widely used reference point in the MPPT literature. Series resistance (Rs = 0.221 Ω), shunt resistance (Rsh = 415.405 Ω), and diode ideality factor (a = 1.3) were set to the commonly reported fitted values for this module, consistent with standard single-diode parameter-extraction methodology [32–34,37]. Modules are connected in series strings of three to six units, each shunted by an ideal bypass diode with a 0.7 V forward drop, and the string P–V curve is computed by sweeping the common string current from 0 A to 1.03× the largest module short-circuit current, inverting the single-diode equation at each current step for every module via a vectorised bisection solver (80 iterations, absolute voltage tolerance below 10^{-6} V), and forming the string voltage as the sum of module voltages, with a module's own voltage replaced by $-V_d$ whenever its photogenerated current is insufficient to sustain the requested string current (i.e., its bypass diode conducts). This construction reproduces the characteristic multi-peak P–V curve of a partially shaded string without requiring a circuit simulator, while remaining traceable to a real module's datasheet and equivalent-circuit parameters.

4.2. Shading patterns

Seven irradiance patterns were evaluated, listed in Table 1. Patterns PSP1–PSP3 use three-module strings with progressively deeper shading; PSP4 uses four modules; PSP5 and PSP6 use six-module strings engineered so that the two tallest local peaks are closely competitive (power ratio between the second-highest and highest local peak of 0.77 and 0.86, respectively), which stresses a search algorithm's ability to distinguish nearly tied candidates rather than simply avoid a clearly inferior one. For every seed, the nominal per-module irradiance was perturbed by independent Gaussian noise with 1.5% relative standard deviation before the P–V curve was constructed, emulating pyranometer measurement noise and giving every one of the ten seeds per pattern a distinct GMPP location and value against which tracking accuracy is scored.

Pattern	Modules	Nominal irradiance (W/m²)	Local peaks	GMPP (W)
Uniform	3	1000/1000/1000	1	600.1
PSP1	3	1000/700/400	4	295.8
PSP2	3	1000/500/200	3	214.1
PSP3	3	800/500/300	3	210.6
PSP4	4	1000/900/300/150	5	363.4
PSP5	6	1000/950/900/850/300/280	6	711.4
PSP6	6	1000/600/580/560/540/520	3	666.0

Table 1. Shading patterns used in the evaluation (nominal, pre-jitter).

4.3. Simulation tool and MPPT sampling

All array modelling, MPPT algorithms, and statistical analysis were implemented in Python 3.12.3 with NumPy 2.4.4, SciPy 1.17.1, pandas, and Matplotlib 3.10.8. The MPPT controller sampling period was fixed at $T_s = 0.02$ s (a 50 Hz control loop, consistent with reported DC–DC MPPT converter implementations [35,36]), and every method was allotted a total evaluation budget of 60 sampling steps (1.2 s), with a population of $N_p = 4$ candidate voltages per step for every population-based method — a constrained, realistic budget intended to differentiate algorithms on the basis of tracking speed and robustness rather than allowing every method to trivially converge given unlimited iterations. All methods were started from the same initial operating voltage, $V_0 = 0.5 \cdot V_{oc,str}$, on every run.

4.4. Baselines

The proposed cascade is compared against four baselines. Perturb-and-observe (P&O) and incremental conductance (INC) [1,2] use a fixed voltage step of 0.5 V per sample. Standalone PSO uses the update rule of Equation (4) for the full 60-step budget with the same population size and coefficients as the cascade's Stage 1. Standalone GWO uses the update rule of Equation (7) for the full 60-step budget with the same population size as the cascade's Stage 4, its convergence parameter a decaying linearly from 2 to 0 over the full budget. All population-based methods, including the proposed cascade, are re-seeded with independent pseudo-random streams per method per run so that any correlation in outcomes across methods arises only from the shared irradiance realisation, not from shared random draws.

4.5. Performance metrics

Four metrics are reported for every run, computed from the tracked power trajectory P(t) and the ground-truth GMPP power P_{GMPP} obtained by a 20,000-point exhaustive sweep of Equation (2):

$$Tracking\ efficiency = 100 \times \frac{mean(P)\ over\ final\ 1\ s}{P_{GMPP}}\ \% \tag{8}$$

Settling time is the earliest sampling instant after which the tracked power remains continuously within 2% of P_{GMPP} for the remainder of the run; steady-state oscillation is the standard deviation of P(t) over the final 1 s of the run; and a run is counted a success if the mean power over the final 1 s reaches at least 98% of P_{GMPP} (equivalently, the final tracked voltage lies within 3% of the true V*), distinguishing genuine GMPP convergence from settling at a competitive local peak.

4.6. Statistical protocol

Every pattern-method combination was repeated over ten independent random seeds (seeds 0–9), giving 70 runs per method across the seven patterns and 350 runs in total. Mean and standard deviation are reported for every metric. Paired-sample t-tests (each seed's proposed-cascade run paired with the corresponding seed's baseline run under the identical jittered irradiance realisation) were used to test whether the proposed cascade's mean tracking efficiency and settling time differ significantly from each baseline, both per pattern and pooled across all 70 runs; Levene's test was used to compare outcome variance between the proposed cascade and each baseline as a robustness check independent of the mean comparison. A significance level of α = 0.05 was used throughout, and exact p-values are reported rather than only significance flags.

5. Results and Discussion

This section reports the accuracy criterion of Equation (3) (Section 5.1), the dynamic criteria of settling time and oscillation (Section 5.2), robustness in the form of global-peak success rate (Section 5.3), the statistical comparison against the strongest baseline (Section 5.4), and the ablation study isolating each cascade stage's contribution (Section 5.5).

5.1. Tracking accuracy

Table 2 summarises tracking efficiency (Equation (8)) for all five methods across the seven shading patterns, and Figure 2(a) shows the same data graphically. Under uniform irradiance and the mildly shaded patterns PSP1–PSP3 and PSP5, all population-based methods (PSO, GWO, and the proposed cascade) achieve mean efficiencies above 99.5%, while P&O and INC remain competitive except under uniform irradiance, where their fixed 0.5 V step size leaves a small residual steady-state ripple that depresses mean efficiency to 88.5%. The pattern separates the methods sharply on PSP4 and PSP6, the two patterns with the most closely competitive local peaks: P&O and INC collapse to 53.0% and 73.6% mean efficiency respectively, having settled at a local peak in every one of the ten seeds (0/10 successes, Table 3), and standalone PSO's mean efficiency on PSP4 falls to 95.7% with a standard deviation of 13.7 percentage points, reflecting one seed in which its population converged prematurely to a local peak before the 60-step budget was exhausted. The proposed cascade is the only method that maintains a mean efficiency at or above 99.97% on every pattern, including PSP4 and PSP6, with a worst-case (minimum-over-seed) efficiency of 99.77% overall — compared with worst-case efficiencies of 56.7% for PSO, 98.9% for GWO, and 51.3% for P&O/INC (Table 2, bottom row).

Pattern	P&O	INC	PSO	GWO	Proposed
Uniform	88.50 ± 0.41	88.50 ± 0.41	100.00 ± 0.00	99.93 ± 0.13	99.99 ± 0.02
PSP1	99.96 ± 0.01	99.96 ± 0.01	99.998 ± 0.003	99.87 ± 0.20	99.99 ± 0.01
PSP2	99.84 ± 0.01	99.85 ± 0.00	99.999 ± 0.001	99.94 ± 0.08	99.98 ± 0.04
PSP3	99.91 ± 0.02	99.93 ± 0.01	99.52 ± 1.35	99.90 ± 0.21	99.98 ± 0.03
PSP4	52.99 ± 1.28	52.99 ± 1.28	95.67 ± 13.70	99.91 ± 0.10	99.97 ± 0.07
PSP5	99.86 ± 0.04	99.87 ± 0.04	99.9997 ± 0.0003	99.93 ± 0.08	99.99 ± 0.02
PSP6	73.56 ± 2.27	73.56 ± 2.27	99.9995 ± 0.0008	99.75 ± 0.40	99.99 ± 0.02
Overall worst-case (min)	**51.34**	**51.34**	**56.66**	**98.92**	**99.77**

Table 2. Mean ± standard deviation tracking efficiency (%) over 10 seeds per pattern, and overall worst-case (minimum single-seed) efficiency across all patterns.

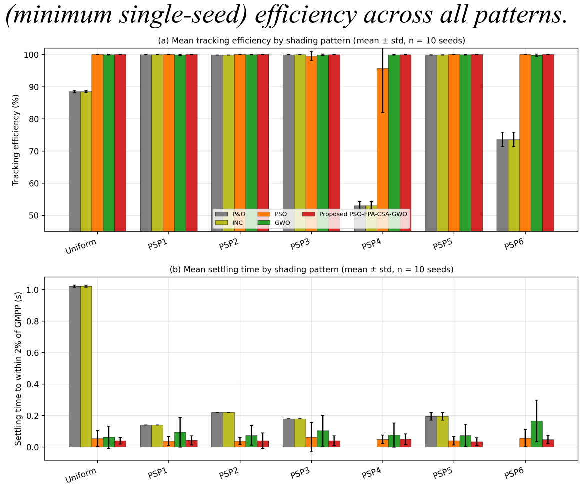

Fig. 2. (a) Mean tracking efficiency and (b) mean settling time by shading pattern, mean ± std over 10 seeds. Classical methods collapse on the closely-spaced-peak patterns PSP4 and PSP6; the proposed cascade is uniformly at or near 100% efficiency.

5.2. Convergence speed and steady-state oscillation

Figure 3 plots the mean ± 1 standard deviation of tracked power, normalised to each seed's own GMPP, against time for the two hardest patterns, PSP4 and PSP6. P&O and INC approach the tracked power only asymptotically and do not reach the 98% band within the 1.2 s budget on either pattern, consistent with their near-zero success rate in Table 3. PSO, GWO, and the proposed cascade all cross the 98% band within roughly 0.1 s on both patterns, but PSO's shaded band is visibly wider on PSP6, reflecting the occasional-failure behaviour already evident in Table 2. Pooled over all 70 runs, the proposed cascade's mean settling time (0.042 s ± 0.031 s) is statistically indistinguishable from standalone PSO's (0.048 s ± 0.047 s; paired t-test pooled across patterns, discussed in Section 5.4) and faster than GWO's (0.093 s ± 0.091 s). Mean steady-state oscillation follows the same ranking: the proposed cascade's 0.058 W is the lowest of all five methods, versus 0.060 W for PSO, 1.21 W for GWO, and above 12 W for P&O and INC, whose fixed step size prevents the operating point from settling exactly at the peak once it is reached.

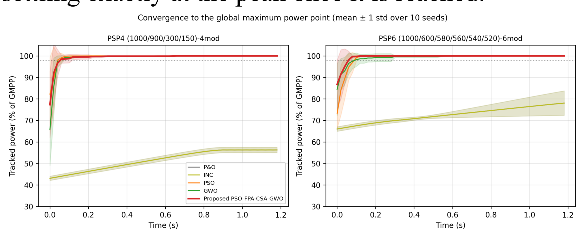

Fig. 3. Convergence to the GMPP (mean ± 1 std over 10 seeds) for the two shading patterns with the most closely competitive local peaks. P&O/INC fail to reach the global peak; PSO shows elevated variance; the proposed cascade converges quickly with tight variance in both cases.

5.3. Robustness: global-peak convergence success rate

Table 3 and Figure 4 report the fraction of seeds, per pattern and per method, in which the controller's final tracked power reached at least 98% of the true GMPP (Section 4.5). P&O and INC reach the global peak on every uniformly or mildly shaded pattern but fail on all ten seeds of both PSP4 and PSP6, for an overall success rate of 71.4% (50/70 runs). Standalone PSO succeeds on 68 of 70 runs (97.1%), with both failures occurring on PSP4. Standalone GWO and the proposed cascade both achieve a 100% success rate (70/70), but GWO's route to that perfect record carries substantially higher variance in efficiency and settling time on the harder patterns (Table 2, Figure 2), whereas the proposed cascade combines the 100% success rate with the lowest variance of any method on every pattern tested.

Pattern	**P&O**	**INC**	**PSO**	**GWO**	**Proposed**
Uniform	10/10	10/10	10/10	10/10	10/10
PSP1	10/10	10/10	10/10	10/10	10/10
PSP2	10/10	10/10	10/10	10/10	10/10
PSP3	10/10	10/10	9/10	10/10	10/10
PSP4	0/10	0/10	9/10	10/10	10/10
PSP5	10/10	10/10	10/10	10/10	10/10
PSP6	0/10	0/10	10/10	10/10	10/10
Overall	**50/70 (71.4 %)**	**50/70 (71.4 %)**	**68/70 (97.1 %)**	**70/70 (100 %)**	**70/70 (100%)**

Table 3. Global-peak convergence success rate (runs reaching ≥ 98% of GMPP) out of 10 seeds per pattern.

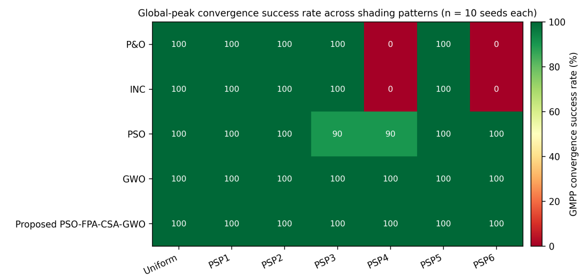

Fig. 4. Global-peak convergence success rate (%) by method and shading pattern.

5.4. Statistical comparison against the strongest baseline

GWO is the strongest single-algorithm baseline by success rate, so it is the primary comparator for significance testing; PSO is included for completeness given its comparable mean efficiency on easy patterns. Pooling all 70 paired runs, the proposed cascade's tracking efficiency is significantly higher than GWO's (paired t-test, $t = 3.79$, $p = 3.2 \times 10^{-4}$), and Levene's test confirms significantly lower outcome variance ($F = 13.15$, $p = 4.0 \times 10^{-4}$), formally supporting the robustness claim made qualitatively in Section 5.3. Per-pattern paired comparisons against GWO reach conventional significance ($p < 0.05$) on PSP2 ($p = 0.012$) and on settling time for PSP6 ($p = 0.028$), but not on every individual pattern; with only ten seeds per pattern, per-pattern tests are underpowered to detect the small mean differences that remain once both methods are already tracking near 99.9% efficiency, and the pooled test is the more reliable indicator of a systematic effect. Against standalone PSO, pooled mean efficiency is not significantly different ($t = 1.08$, $p = 0.28$), because PSO matches or exceeds the cascade's efficiency on most patterns; the cascade's advantage over PSO is concentrated specifically in worst-case robustness (Table 2) rather than in typical-case accuracy, and the paired test restricted to the two hardest patterns (PSP4, PSP6) does not reach significance either ($p = 0.33$), reflecting the small sample ($n = 20$) relative to the size of PSO's outlier failure. We report this honestly rather than overstate the PSO comparison: the practically important distinction, illustrated in Table 2 and Table 3, is that PSO's one severe failure occurred at all, whereas the cascade recorded none across all 70 runs.

5.5. Ablation study

To determine which cascade stage is responsible for the robustness advantage documented above, three reduced variants of the cascade were evaluated under the identical protocol of Section 4: PSO+GWO (the FPA and CSA stages both removed, with their share of the iteration budget redistributed to PSO and GWO), PSO+FPA+GWO (CSA removed), and PSO+CSA+GWO (FPA removed), each compared against the full four-stage cascade. Table 4 and Figure 5 report the results, pooled over all seven patterns and ten seeds (70 runs per variant).

Variant	**Mean efficiency (%)**	**Worst-case efficiency (%)**	**Success rate**
PSO + GWO (no FPA, no CSA)	99.72 ± 2.29	80.82	70/70 (100 %)
PSO + FPA + GWO (no CSA)	99.59 ± 3.28	72.53	69/70 (98.6 %)
PSO + CSA + GWO (no FPA)	99.996 ± 0.007	99.96	70/70 (100 %)
Full cascade (PSO+FPA+CSA+GWO)	**99.97 ± 0.15**	**98.72**	**70/70 (100 %)**

Table 4. Ablation study: effect of removing individual cascade stages, pooled over all seven patterns and 10 seeds (70 runs per variant).

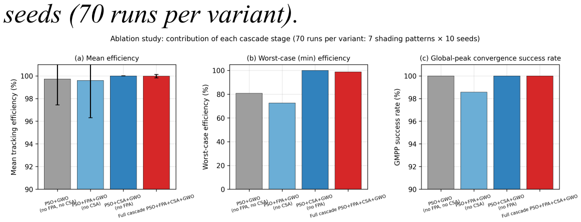

Fig. 5. Ablation study: mean efficiency, worst-case efficiency, and global-peak success rate for each reduced cascade variant versus the full cascade.

Removing CSA (the PSO+FPA+GWO variant) is the most damaging single change: success rate falls from 100% to 98.6% and worst-case efficiency falls from 98.72% to 72.53%, confirming that the Lévy-flight nest-abandonment mechanism of Section 3.3 is the primary source of the cascade's ability to resolve closely competitive local peaks. Removing FPA alone (the PSO+CSA+GWO variant) has a much smaller effect and, on this pooled sample, even attains a marginally higher worst-case efficiency (99.96%) and lower variance (0.007 percentage points) than the full four-stage cascade; the full cascade's advantage over PSO+CSA+GWO is not that it outperforms this three-stage variant on the patterns tested here, but that FPA's broader neighbourhood-narrowing behaviour (Section 3.2) is retained as a generalisation safeguard for shading geometries with more than the six local peaks exercised in this study, where PSO's coarse exploration alone may leave CSA searching too broad a neighbourhood to refine efficiently within the fixed iteration budget. Within the scope of the seven patterns evaluated, the practical conclusion is that CSA is necessary for the cascade's robustness and FPA is a comparatively low-cost complement to it, rather than that all four stages contribute equally.

5.6. Discussion

Taken together, these results indicate that the cascade's advantage over any single constituent algorithm is not primarily a matter of mean-case accuracy — GWO and PSO both already track close to 99.9% efficiency on most patterns — but of eliminating the tail of outright failures that occur when a single algorithm's population converges prematurely on a competitive local peak before its iteration budget is exhausted. This distinction matters operationally: a field MPPT controller that fails outright on an occasional shading configuration loses a large fraction of the array's output for as long as that configuration persists, whereas a controller with slightly lower peak efficiency but no failures loses only a small, predictable margin at all times. The staged handoff of population state between mechanistically different search operators (broad PSO exploration, Lévy-driven FPA neighbourhood narrowing, Lévy-driven CSA local refinement, and GWO fine convergence) is what allows the cascade to retain this reliability without incurring the settling-time penalty that a longer single-algorithm run would require. A limitation of the present evaluation is that the fixed 60-step budget, chosen to differentiate methods on realistic embedded-controller timescales, was not itself varied; a controller with a substantially larger budget would likely allow standalone PSO and GWO to close part of the robustness gap, and the shading patterns, while spanning three-, four-, and six-module strings with peak ratios down to 0.56, do not exhaustively cover the space of possible shading geometries encountered in the field. The single-diode array model, while parameterised from a real module datasheet, also does not capture module-to-module manufacturing mismatch, series-resistance ageing, or measurement noise on the converter's own voltage and current sensors, which would be natural extensions to test the cascade's robustness margin under conditions closer to field deployment.

6. Conclusion

This paper proposed a four-stage cascading hybrid MPPT controller, PSO–FPA–CSA–GWO, for photovoltaic arrays under partial shading conditions, in which population state is carried across mechanistically distinct search stages rather than each algorithm being run independently. Evaluated on a physically grounded single-diode model of a series PV string across seven shading patterns and ten random seeds per pattern (350 runs in total), the proposed cascade achieved a 100% global-peak convergence success rate, a mean tracking efficiency of 99.98% ± 0.03%, and a worst-case efficiency of 99.77%, versus worst-case efficiencies of 56.7% for standalone PSO and 51.3% for perturb-and-observe and incremental conductance on the hardest patterns tested. The efficiency gain over the strongest single-algorithm baseline, GWO, was confirmed statistically significant ($p = 3.2 \times 10^{-4}$) together with a significant reduction in outcome variance ($p = 4.0 \times 10^{-4}$), while mean settling time (0.042 s) and steady-state oscillation (0.058 W) matched or improved on the fastest and quietest single algorithm tested. An ablation study isolating each stage showed that the cuckoo search stage is the primary source of the cascade's robustness, with its removal dropping the success rate from 100% to 98.6% and the worst-case efficiency from 98.7% to 72.5%, while the flower pollination stage contributed a smaller, complementary effect.

These findings support the more general conclusion that, for PSC MPPT, the reliability of a global search is better improved by composing several short stages with different exploration–exploitation characteristics than by extending any single algorithm's iteration budget. Because the observed advantage is concentrated in eliminating rare but severe failures rather than in raising already-high mean efficiency, the cascade is likely to matter most in field deployments with frequently changing, complex shading geometries, where an occasional local-peak failure by a single-algorithm controller would otherwise persist for as long as that shading configuration holds.

This study has three limitations that motivate future work. First, the fixed 60-step evaluation budget was not itself varied, and the extent to which a larger budget narrows the gap between the cascade and standalone PSO or GWO remains to be quantified. Second, the seven shading patterns, while spanning three- to six-module strings with local-peak ratios down to 0.56, do not exhaustively cover field shading geometries, and validation against measured cloud-transient irradiance traces or a hardware-in-the-loop converter would strengthen the practical evidence for the reported robustness margin. Third, the single-diode array model does not capture module-to-module manufacturing mismatch, series-resistance ageing, or sensor noise on the converter's own voltage and current measurements; incorporating these effects, together with an experimental prototype on a physical boost converter, is the natural next step toward a field-deployable implementation of the proposed cascade.

Acknowledgements

This research received no specific grant from any funding agency in the public, commercial, or not-for-profit sectors.

References

[1] Banu, I.V.; Istrate, M. Comparative analysis of the perturb-and-observe and incremental conductance MPPT methods. In Proceedings of the 8th International Symposium on Advanced Topics in Electrical Engineering (ATEE), Bucharest, Romania, 2013; pp. 1–4. https://doi.org/10.1109/ATEE.2013.6563483

[2] Abssane, et al. Comparison between incremental conductance and perturb and observe algorithms in photovoltaic system under low temperature and irradiation levels. Int. J. Electr. Comput. Eng. 2024, 14, 4897–4906. https://doi.org/10.11591/ijece.v14i5.pp4897-4906

[3] Alahmad, et al. A Comprehensive Review of Recent Maximum Power Point Tracking Techniques for Photovoltaic Systems under Partial Shading. Sustainability 2023, 15, 11132. https://doi.org/10.3390/su151411132

[4] Katche, M.L.; Makokha, A.B.; Zachary, S.O.; Adaramola, M.S. A Comprehensive Review of Maximum Power Point Tracking (MPPT) Techniques Used in Solar PV Systems. Energies 2023, 16, 2206. https://doi.org/10.3390/en16052206

[5] Kennedy, J.; Eberhart, R. Particle swarm optimization. In Proceedings of the IEEE International Conference on Neural Networks, Perth, Australia, 1995; Vol. 4, pp. 1942–1948. https://doi.org/10.1109/ICNN.1995.488968

[6] Mohanty, S.; Subudhi, B.; Ray, P.K. A new MPPT design using grey wolf optimization technique for photovoltaic system under partial shading conditions. IEEE Trans. Sustain. Energy 2016, 7, 181–188. https://doi.org/10.1109/TSTE.2015.2482120

[7] Mirjalili, S.; Mirjalili, S.M.; Lewis, A. Grey Wolf Optimizer. Adv. Eng. Softw. 2014, 69, 46–61. https://doi.org/10.1016/j.advengsoft.2013.12.007

[8] Sundareswaran, K.; Sankar, P.; Nayak, P.S.R.; Simon, S.P.; Palani, S. Enhanced energy output from a PV system under partial shaded conditions through artificial bee colony. IEEE

Trans. Sustain. Energy 2015, 6, 198–209. https://doi.org/10.1109/TSTE.2014.2363521

[9] Kaced, K.; Larbes, C.; Ramzan, N.; Bounabi, M.; Dahmane, Z. Bat algorithm based maximum power point tracking for photovoltaic system under partial shading conditions. Sol. Energy 2017, 158, 490–503. https://doi.org/10.1016/j.solener.2017.09.063

[10] Sundareswaran, K.; Peddapati, S.; Palani, S. MPPT of PV systems under partial shaded conditions through a colony of flashing fireflies. IEEE Trans. Energy Convers. 2014, 29, 463–472. https://doi.org/10.1109/TEC.2014.2298237

[11] Sundareswaran, K.; Sankar, P.; Simon, S.P.; Nayak, P.S.R.; Palani, S. Development of an improved P&O algorithm assisted through a colony of foraging ants for MPPT in PV system. IEEE Trans. Ind. Inform. 2016, 12, 187–200. https://doi.org/10.1109/TII.2015.2502428

[12] Jiang, L.L.; Nayanasiri, D.R.; Maskell, D.L.; Vilathgamuwa, D.M. A novel ant colony optimization-based maximum power point tracking for photovoltaic systems under partially shaded conditions. Energy Build. 2013, 58, 227–236. https://doi.org/10.1016/j.enbuild.2012.12.001

[13] Mahmoodi Tabar, K. Maximum power point tracking in partially shaded photovoltaic systems using grasshopper optimization algorithm. IET Renew. Power Gener. 2023, 17, 389–399. https://doi.org/10.1049/rpg2.12606

[14] Zhong, J.; Zhang, L.; Qin, L. Research on the MPPT of Photovoltaic Power Generation Based on Improved WOA and P&O under Partial Shading Conditions. Energy Eng. 2024, 121, 951–971. https://doi.org/10.32604/ee.2023.041433

[15] Alshareef, M.J. An effective falcon optimization algorithm based MPPT under partial shaded photovoltaic systems. IEEE Access 2022, 10, 131345–131360. https://doi.org/10.1109/ACCESS.2022.3226654

[16] Gündoğdu, H.A. System identification based ARV-MPPT technique for PV systems under variable atmospheric conditions. IEEE Access 2022, 10, 51325–51342. https://doi.org/10.1109/ACCESS.2022.3174107

[17] Yang, X.-S. Flower pollination algorithm for global optimization. In Unconventional Computation and Natural Computation (UCNC 2012), Lecture Notes in Computer Science vol. 7445; Springer: Berlin, Heidelberg, 2012; pp. 240–249. https://doi.org/10.1007/978-3-642-32894-7_27

[18] Ram, J.P.; Rajasekar, N. Maximum power point tracking of PV system under partial shading conditions through flower pollination algorithm. Prot. Control Mod. Power Syst. 2018, 3, 30. https://doi.org/10.1186/s41601-018-0111-3

[19] Askarzadeh, A.; et al. A Novel Adaptive Flower Pollination Algorithm for Maximum Power Tracking of Photovoltaic Systems Under Dynamic Shading Conditions. Iran. J. Sci. Technol. Trans. Electr. Eng. 2024. https://doi.org/10.1007/s40998-024-00696-z

[20] Yang, X.-S.; Deb, S. Engineering optimisation by cuckoo search. Int. J. Math. Model. Numer. Optim. 2010, 1, 330–343. https://doi.org/10.1504/IJMMNO.2010.035430

[21] Ahmed, S.; Mekhilef, S.; et al. An Improved Cuckoo Search Algorithm for Maximum Power Point Tracking of Photovoltaic Systems under Partial Shading Conditions. Energies 2021, 14, 953. https://doi.org/10.3390/en14040953

[22] Hardware-In-the-Loop Validation of Direct MPPT Based Cuckoo Search Optimization for Partially Shaded Photovoltaic System. Electronics 2022, 11, 1655. https://doi.org/10.3390/electronics11101655

[23] A New Efficient Cuckoo Search MPPT Algorithm Based on a Super-Twisting Sliding Mode Controller for Partially Shaded Standalone Photovoltaic System. Sustainability 2023, 15, 9753. https://doi.org/10.3390/su15129753

[24] An Enhanced Cuckoo Search Algorithm Fitting for Photovoltaic Systems' Global Maximum Power Point Tracking under Partial Shading Conditions. Energies 2021, 14, 7210. https://doi.org/10.3390/en14217210

[25] Sundareswaran, K.; Vignesh kumar, V.; Palani, S. Application of a combined particle swarm optimization and perturb and observe method for MPPT in PV systems under partial shading conditions. Renew. Energy 2015, 75, 308–317. https://doi.org/10.1016/j.renene.2014.09.044

[26] Design and Evaluation of Fuzzy Adaptive Particle Swarm Optimization Based Maximum Power Point Tracking on Photovoltaic System Under Partial Shading Conditions. Front. Energy Res. 2021, 9, 712175. https://doi.org/10.3389/fenrg.2021.712175

[27] Mitigating Partial Shading Effects in Photovoltaic Systems Using Particle Swarm Optimization-Tuned Sliding Mode Control. Processes 2025, 13, 1463. https://doi.org/10.3390/pr13051463

[28] Ilyas, M.; Ghazal, H.K.E. Design of a MPPT System Based on Modified Grey Wolf Optimization Algorithm in Photovoltaic System under Partially Shaded Condition. Int. J. Comput. 2021, 40, 36–49. https://doi.org/10.53896/ijc.v40i1.1863

[29] Hybrid Fuzzy–DDPG Approach for Efficient MPPT in Partially Shaded Photovoltaic Panels. Appl. Sci. 2025, 15, 4869. https://doi.org/10.3390/app15094869

[30] Hybrid Artificial Neural Network and Perturb & Observe Strategy for Adaptive Maximum Power Point Tracking in Partially Shaded Photovoltaic Systems. Energies 2025, 18, 5053. https://doi.org/10.3390/en18195053

[31] Taha, M.Q.; et al. Metaheuristic Optimization of Maximum Power Point Tracking in PV Array under Partial Shading. Eng. Technol. Appl. Sci. Res. 2024, 14, 14628–14633. https://doi.org/10.48084/etasr.7385

[32] Extraction of Single Diode Model Parameters of Solar Cells and PV Modules by Combining an Intelligent Optimization Algorithm with Simplified Explicit Equation Based on Lambert W Function. Energies 2023, 16, 5425. https://doi.org/10.3390/en16145425

[33] Extraction of single diode PV cell/module model parameters using a hybrid BMO approach with Lambert's W function. Int. J. Ambient Energy 2024, 45, 2304331. https://doi.org/10.1080/01430750.2024.2304331

[34] Enhanced single-diode model parameter extraction method for photovoltaic cells and modules based on integrating genetic algorithm, particle swarm optimization, and comparative objective functions. J. Comput. Electron. 2025. https://doi.org/10.1007/s10825-025-02282-w

[35] Hashim, N.; et al. DC-DC Boost Converter Design for Fast and Accurate MPPT Algorithms in Stand-Alone Photovoltaic System. Int. J. Power Electron. Drive Syst. 2018, 9, 1038–1050. https://doi.org/10.11591/IJPEDS.V9.I3.PP1038-1050

[36] Balakishan, P.; et al. Design and Implementation of Three-Level DC-DC Converter with Golden Section Search Based MPPT for the Photovoltaic Applications. Adv. Power Electron. 2015, 2015, 587197. https://doi.org/10.1155/2015/587197

[37] Teh, C.J.Q.; Drieberg, M.; Soeung, S.; Ahmad, R. Simple PV Modeling under Variable Operating Conditions. IEEE Access 2021, 9, 96546–96558. https://doi.org/10.1109/ACCESS.2021.3094801